Journal of Alloys and Compounds 834 (2020) 154952

Contents lists available at ScienceDirect

Journal of Alloys and Compounds

journal homepage: http://www.elsevier.com/locate/jalcom

# Influence of alloying elements, in-situ dispersoids and fabrication on microstructure and properties of W-(Ta,V,Ti) ODS alloys

Chun-Liang Chen [a, *], Sutrisna [a, b]

[a] Department of Materials Science & Engineering, National Dong Hwa University, Shou-Feng, Hualien, 97401, Taiwan
[b] Department of Mechanical Engineering, Institut Teknologi Nasional, Yogyakarta, 55281, Indonesia

ARTICLE INFO

*Article history:*
Received 17 January 2020
Received in revised form
15 March 2020
Accepted 25 March 2020
Available online 4 April 2020

*Keywords:*
Tungsten alloy
Oxide dispersion strengthening
Mechanical alloying
Plasma facing materials

ABSTRACT

In this study, the effect of Ta, V and Ti in W matrix on characteristics and synthesis of the model alloys were investigated. The secondary ball milling method and in-situ Y dispersed oxides were used to further improve material properties. The results showed that the model alloys adding with the V element could facilitate the grain refinement and microstructure homogeneity of the tungsten alloys. The (Ta,V)-rich and V-rich oxides were found in the microstructure and have been identified as the $TaVO_4$ and $V_2O_5$ phases. The nano-scale of the in-situ oxide particle $YTaO_4$ was observed and coherent with the tungsten matrix. Moreover, the secondary ball milling method was effective to refine the microstructure and to increase the relative density and mechanical properties.



## 1. Introduction

Tungsten alloys are considered prime candidates for plasma facing materials (PFMs) in fusion devices due to their attractive combinations of high radiation resistance, low neutron activation, high sputtering threshold, high strength at elevated temperature, low thermal expansion, high thermal conductivity and great corrosion resistance [1–3]. However, tungsten alloys have critical drawbacks for structural applications including high ductile-brittle transition temperature (DBTT), low recrystallization temperature, and material brittleness due to grain boundary impurities [4,5].

In the last decades, a lot of research has been done towards the design of plasma facing materials to improve the ductility, mechanical properties, and fine grain microstructure of tungsten alloys by alloying with other elements such as Ti, V, Ta, Re or adding oxide dispersion-strengthened (ODS) particles like $Y_2O_3$ or $La_2O_3$ through mechanical alloying technique [6–9]. The presence of V and Ta elements in the tungsten matrix can improve the densification, morphology and mechanical properties as well as reduces the irradiation embrittlement of the materials [10–12]. Moreover, the addition of Ta in tungsten contributes to the refinement of microstructure and resistance to crack growth [13–15]. Most significant enhancement of W–Ta alloys may be in regards to hydrogen isotope retention [15]. Addition of Ti acts as a sintering activator and improves the densification of materials [16]. Ti addition also alters the slip mechanism and thus increases the ductility of tungsten-based alloys [16].

In earlier work [17–20], we investigated the effect of Ti contents on W–Ti alloys and also studied on W–Ti alloys dispersed with the different reinforcement particles ($Y_2O_3$, $Y_2Ti_2O_7$, in-situ La oxides) and the different consolidation methods. In this current study, a further investigation was carried out to examine the influence of alloying elements (V, Ta, Ti) and the different milling methods by mechanical alloying. Moreover, we also studied on the effect of the rare earth element Y on microstructural evolution and mechanical properties of tungsten model alloys. It is important to understand the role of alloying elements and in-situ formed dispersoids in tungsten alloys and how they interact with tungsten matrix. A secondary ball milling method was also introduced in this work to improve the synthesis of the tungsten alloys. The aim of this work is to develop high performance tungsten-based alloys for plasma facing materials' applications.

## 2. Experimental procedure

Pure W, Ti, V, Ta and rare earth element of Y powders used as the starting materials. The particles size for all of elemental powders

* Corresponding author. No. 1, Sec. 2, Da Hsueh Rd., Shoufeng, Hualien, 97401, Taiwan.
*E-mail address:* chunliang@gms.ndhu.edu.tw (C.-L. Chen).

https://doi.org/10.1016/j.jallcom.2020.154952
0925-8388/

with 99.9% of purity are in the range of 5–50 μm. The four-tungsten model alloys with the different alloying elements synthesized by different milling methods were studied and named as W–Ta–V_S, W–Ti–Ta_S, W–Ti–V_S, and W–Ta–V_P. The details of the chemical composition and milling methods of the model alloys are given in Table 1. The samples prepared by the secondary ball milling method are carried out through two-stages of mechanical alloying. The first stage, tungsten and yttrium powders are pre-milled as a matrix for 8 h. Further, the matrix and alloying powders (Ta, Ti, V) were milled again for 4, 8, 12, and 20 h. Mechanical alloying was carried out in the planetary ball mill (Retsch PM100) with 350 rpm of speed under an argon atmosphere for different milling time. Ball milling process employed a tungsten carbide medium (vials and balls) with the ball to powder ratio (BPR) of 10:1. The process control agent (PCA) stearic acid (0.5 wt%) has been used to inhibit agglomeration of powders during ball milling. The milled powders were consolidated by uniaxial cold pressing into green compacts with a pressure of 210 MPa in 15 s. The samples in the shape of discs (diameter of 5 mm and thickness of 2–3 mm) were received after the conventional consolidation process. The green compacted samples were then sintered at 1450 °C for 1 h under atmospheric pressure with a mixed hydrogen-argon atmosphere. The heating rate of 2 °C/min was used as the sintering temperature increases from 950 to 1450 °C. The samples were cooled to room temperature at the cooling rate of 2–5 °C/min. The microstructure and chemical composition of the model alloys were characterized by X'Pert PRO X-ray diffractometer (XRD) and a Hitachi-4700 SEM with energy-dispersive X-ray spectroscopy (EDS). Phase identification and crystal structure of the complex oxides were further analyzed by a FEI Tecnai F20 G2 file emission gun transmission electron microscope (TEM) operating at 200 KeV. The crystallite size and lattice strain were estimated using Scherrer's formula as follows [21].

$$B_r = \frac{0.9\lambda}{t\cos\theta} + \eta\tan\theta$$

where $B_r$ is the total broadening due to crystal refining and lattice strains; $\lambda$ is the X-ray wave length; $t$ is the crystallite size, $\theta$ is the Bragg angle and $\eta$ is the strain in the material. The Vickers hardness measurements were performed at room temperature by using a 1 kg load for 15 s. The nanoindentation tests (MTS Nanoindenter XP) were conducted to obtain indentation hardness and elastic modulus using the continuous stiffness measurement (CSM) method. Meanwhile, the relative density was measured using the Archimedes method.

## 3. Results and discussion

### 3.1. Characterization of the milled powders

Fig. 1 shows the XRD spectra of the W–Ta–V_S alloyed powders as a function of milling time. The main peaks of W along with very small peaks of Ta and V elements were clearly detected in the unmilled powders. However, after 4 h of milling, the reflection peaks of Ta and V were disappeared, suggesting that Ta and V atoms dissolved into the W crystalline lattice and lead to the formation of a solid solution during mechanical alloying. It was also found that the XRD peaks showed reduction in peak intensity and broadening of peak with the milling time increasing, which was related to grain refinement and lattice distortions.

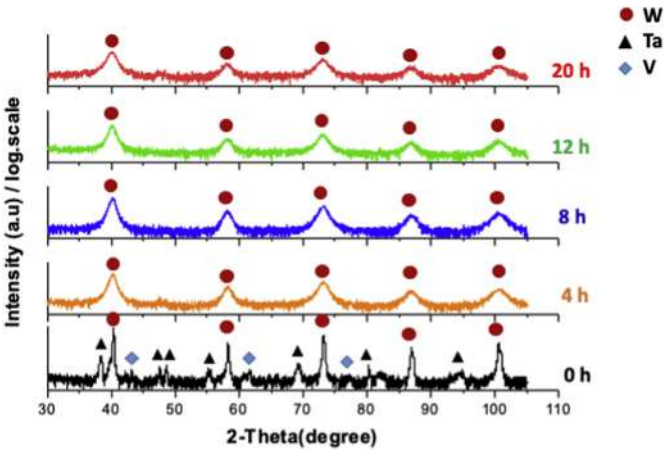


**Fig. 1.** XRD spectra of W–Ta–V_S powders milled for different milling durations: 4, 8, 12 and 20 h.

Fig. 2 shows the change of the crystallite size and lattice distortion of the W–Ta–V_S alloyed powders as a function of milling time. It can be seen clearly that the crystallite size decreases rapidly at the early stage of milling and approaches to 10 nm at 20 h of milling. The high-energy impacts during ball milling not only decrease the crystallite size but also increase the lattice strain as shown in Fig. 2. A high lattice distortion was generated after prolonged milling (20 h), resulting in a large number of crystal defects formed at the milled powders such as dislocations, vacancies, twin faults, and stacking faults [8].

### 3.2. Characterization of the sintered model alloys

#### 3.2.1. SEM observation and EDS analysis

Fig. 3 shows the SEM-BSE images of the W–Ta–V_S model alloys milled for 4, 8, 12 and 20 h by a secondary ball milling method. At the initial stages of milling (see Fig. 3a and b), large number of small dark particles (less than 1 μm) were obtained and non-uniformly distributed in the tungsten matrix. As the milling time increased to 12 h and 20 h, see Fig. 3c and d, a larger size of dark particles (~5 μm) containing a high concentration of C, O, V and Ta

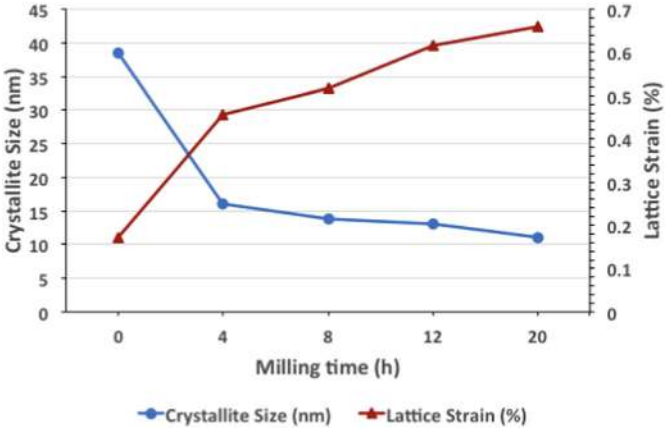


**Fig. 2.** Variation of crystallite size and lattice distortion of the W–Ta–V_S powders as a function of milling time.

**Table 1**
Chemical composition of the four model alloys (wt.%).

| Model alloys | W | Ta | Ti | V | Y | Milling methods |
|---|---|---|---|---|---|---|
| W–Ta–V_S | Bal. | 2 | – | 2 | 0.5 | Secondary |
| W–Ti–Ta_S | Bal. | 2 | 2 | – | 0.5 | Secondary |
| W–Ti–V_S | Bal. | – | 2 | 2 | 0.5 | Secondary |
| W–Ta–V_P | Bal. | 2 | – | 2 | 0.5 | Primary |

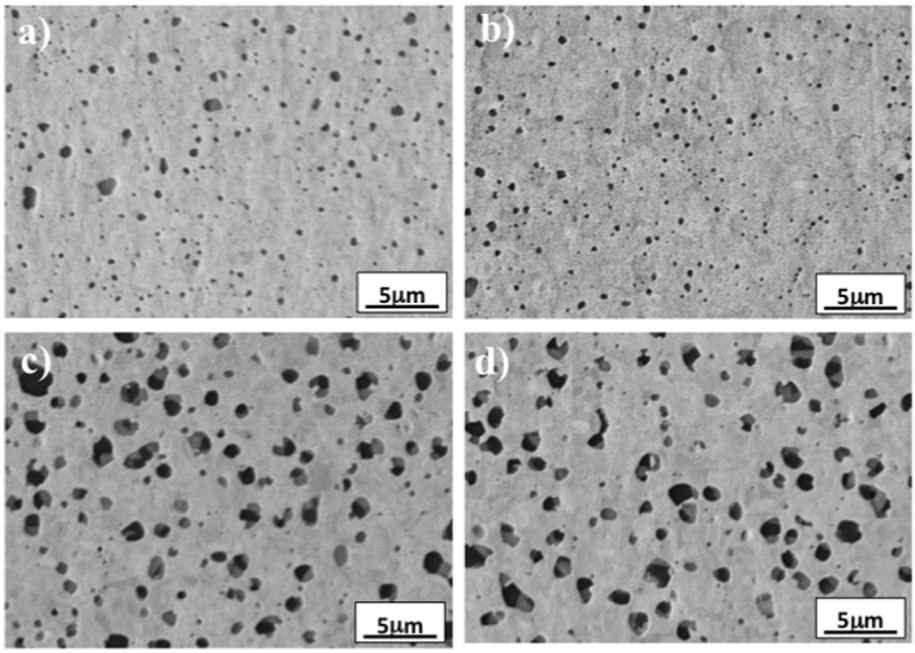


**Fig. 3.** SEM images of the sintered W–Ta–V_S samples secondarily milled for (a) 4 h, (b) 8 h, (c) 12 h and (d) 20 h.

elements was observed and uniformly dispersed in the tungsten matrix. It suggests that Ta and V have greater affinity for oxygen or carbon and thereby contamination (e.g., C, O etc.) during the ball milling and high temperature sintering can promote the formation of (V,Ta)-rich oxides or carbides.

Fig. 4 shows the microstructure of the four different tungsten model alloys. The SEM-BSE images of the W–Ta–V_S, W–Ti–Ta_S and W–Ti–V_S model alloys milled for 20 h by the secondary ball milling can be seen in Fig. 4a–c. In the W–Ta–V_S sample, see Fig. 4a, a large number of particles appearing as a dark area were found in the microstructure, which contain a high concentration of Ta, V and O elements. The (Ta,V)-rich oxide with dark gray contrast and the V-rich oxide with black contrast have been confirmed by EDS, see the points "A" and "B". However, a large size of an irregular shape particle (~5 μm) was observed at the W–Ti–Ta_S sample as shown in Fig. 4b. The large particles have been identified as the Ti-rich oxide (see the point "C" for the black particle) or the (Ta,Ti)-rich oxide (see the point "D" for the dark gray particle). In case of the W–Ti–V_S model alloy, it demonstrates the formation of a small particle with black contrast, which indicates as the (Ti,V)-rich oxide as shown in Fig. 4c at the point "E". On the contrary, Fig. 4d shows the W–Ta–V_P model alloy fabricated by the primary ball milling. It exhibits a large grain structure with a non-uniform distribution of the large particles. In this case, the (Ta,V)-rich oxide and V-rich oxide have been identified by EDS analysis as shown in Fig. 4d at the points "F" and "G". Determined chemical composition of each

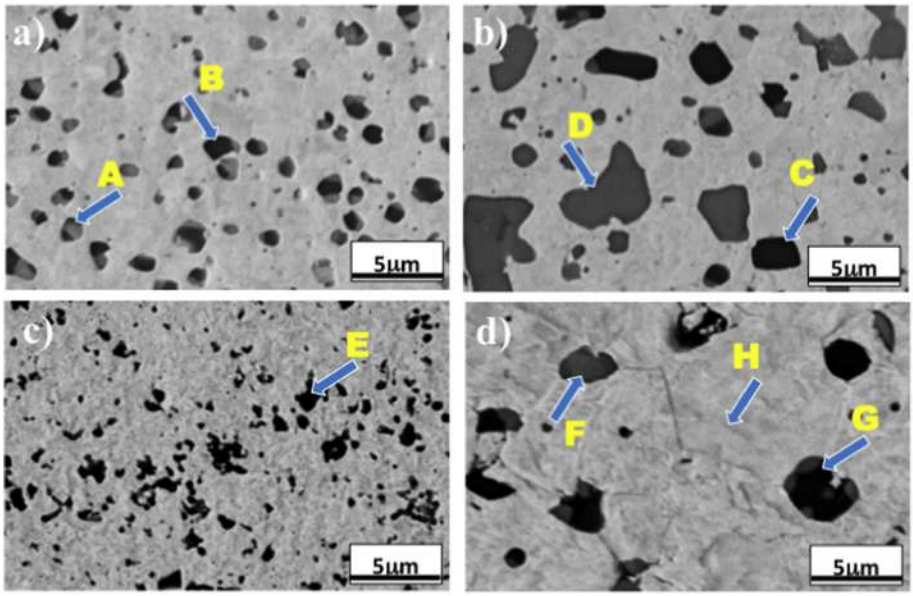


**Fig. 4.** SEM images of the sintered (a) W–Ta–V_S, (b) W–Ti–Ta_S (c) W–Ti–V_S, (d) W–Ta–V_P model alloys milled for 20 h.

**Table 2**
EDX analysis of the model alloys showing in Fig. 4. (wt.%).

| Element | W | Ta | V | Ti | O | C |
|---|---|---|---|---|---|---|
| Point A | 16.38 | 36.37 | 26.63 | – | 19.62 | – |
| Point B | – | – | 70.26 | – | 29.74 | – |
| Point C | – | – | – | 59.22 | 40.78 | – |
| Point D | 8.08 | 43.36 | – | 25.10 | 23.46 | – |
| Point E | – | – | 29.38 | 52.78 | 17.85 | – |
| Point F | 15.65 | 36.28 | 27.43 | – | 20.63 | – |
| Point G | – | – | 58.94 | – | 41.06 | – |
| Point H | 85.94 | – | – | – | – | 14.06 |

point in the different model alloys by EDS analysis is listed in Table 2.

According to the SEM-EDS results, see Fig. 4 and Table 2, there are several interesting findings about effects of alloying elements and milling processing on microstructure development that should be emphasized. First of all, the addition of Ti can promote the formation of a large size of Ti-rich oxide particles, as shown in Fig. 4b. It is believed that the reactive Ti powder could create an increase in surface energy and residual oxygen contamination during ball milling facilitates the nucleation sites for the formation of titanium oxides. The subsequent high temperature sintering can further accelerate the rapid growth of titanium oxides formed on the tungsten matrix. Secondly, the presence of V element can refine the second phase particles with a uniform distribution as shown in Fig. 4a and c. It has been suggested that Ta and V elements in W matrix could facilitate a uniform distribution of particles on the microstructure for tungsten alloys [10,11]. Furthermore, Ta addition seems to change the morphology of oxide particles from an irregular shape to a more spherical shape. Thirdly, in comparison between the W–Ta–V_S and W–Ta–V_P model alloys, see Fig. 4a and d, it is believed that the different milling method strongly influences the size and distribution of the secondary phase particles and microstructure evolution. It can be seen clearly that the secondary ball milling can lead to the grain refinement and the uniform distribution of fine oxide particles as shown in Fig. 4a. In additional, tungsten matrix also contains a small amount of carbon content, implying contamination created from grinding media using tungsten carbide vial and balls [22].

Fig. 5 shows EDS mapping images of the W–Ta–V_S model

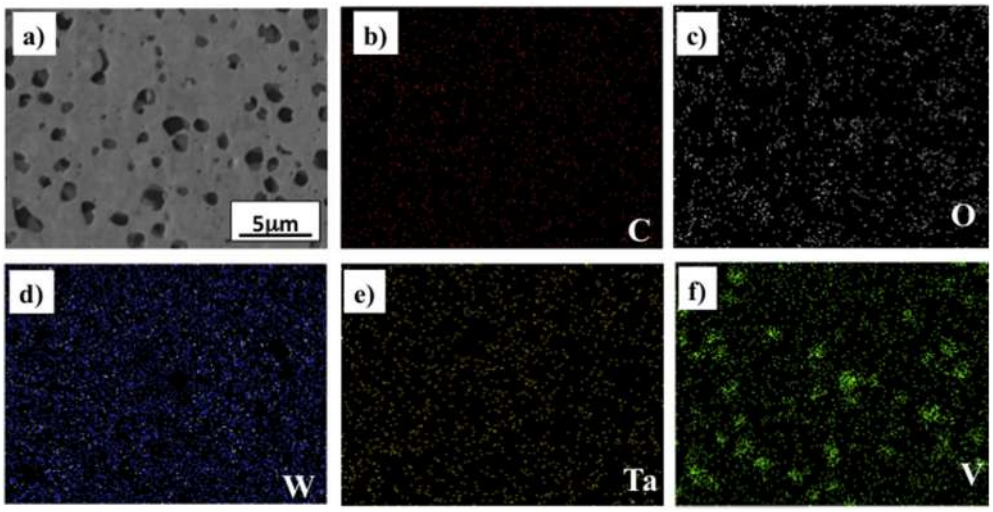


**Fig. 5.** EDS mapping of the W–Ta–V_S sample milled for 20 h and sintered; (a) SEM image, (b) C map, (c) O map, (d) W map, (e) Ta map and (f) V map.

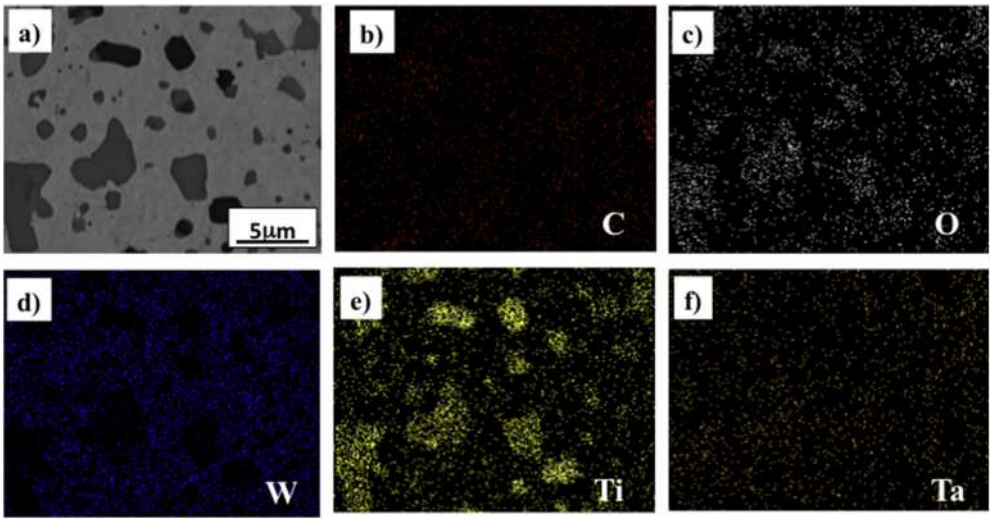


**Fig. 6.** EDS mapping of the W–Ti–Ta_S sample milled for 20 h and sintered; (a) SEM image, (b) C map, (c) O map, (d) W map, (e) Ta map and (f) V map.

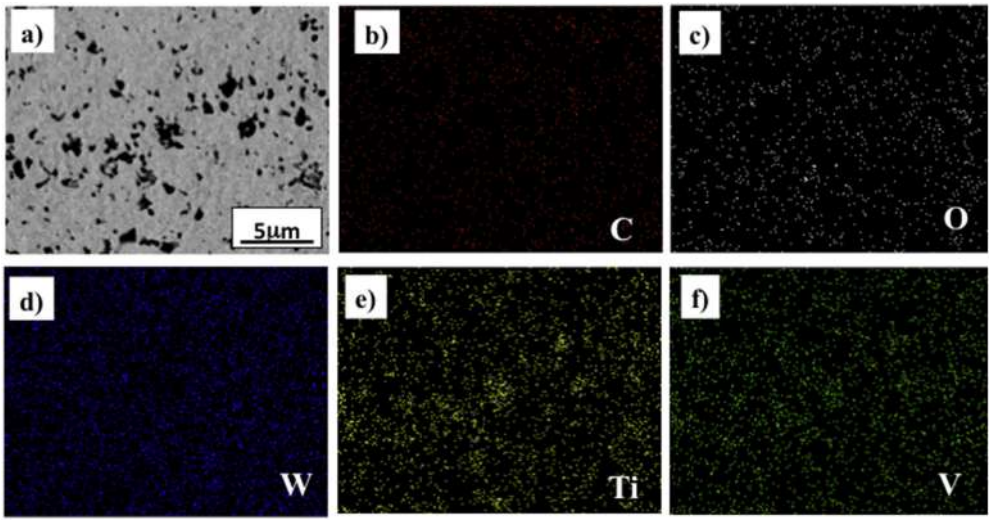


**Fig. 7.** EDS mapping of the W—Ti—V_S sample milled for 20 h and sintered; (a) SEM image, (b) C map, (c) O map, (d) W map, (e) Ta map and (f) V map.

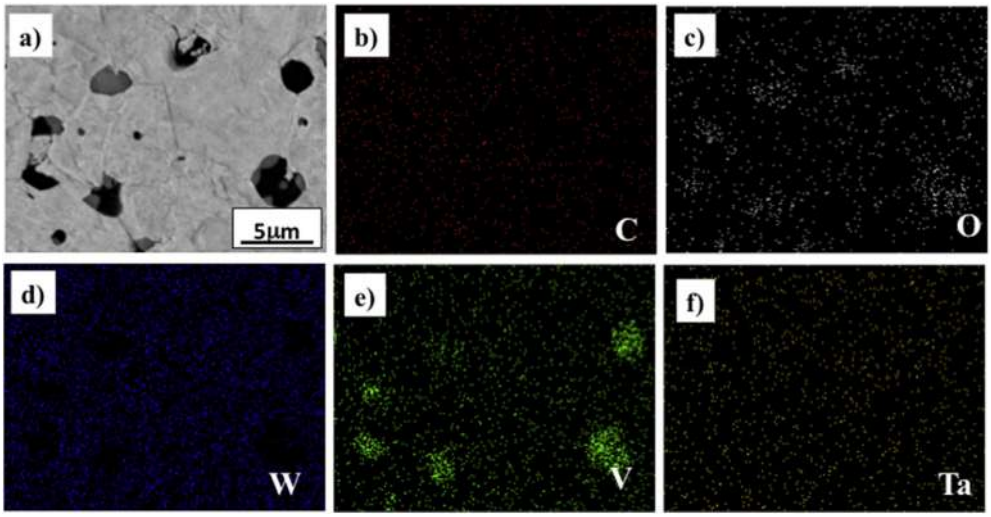


**Fig. 8.** EDS mapping of the W—Ta—V_P sample milled for 20 h and sintered; (a) SEM image, (b) C map, (c) O map, (d) W map, (e) Ta map and (f) V map.

alloy. The maps of W, Ta and C reveal a homogeneous distribution of elements in the microstructure; however, the V and O maps display noticeable segregation. This corresponds to the formation of V-rich oxides appeared as small particles in the microstructure as shown in SEM image (Fig. 4a). Figs. 6–8 also demonstrate EDS mapping images of the W—Ti—Ta_S, W—Ti—V_S and W—Ta—V_P model alloys. The results indicate that Ti has a high reactivity with oxygen atoms and thereby Ti-rich oxides have been often found in Ti-containing alloys fabricated by the mechanical alloying rote [17]. It can be concluded that in this study, Ti and V have greater affinity for oxygen and promote the formation of Ti-rich or V-rich oxides during ball milling process or subsequent high temperature sintering.

### 3.2.2. TEM investigation

TEM techniques were further used to investigate the crystal structure of the second phases formed in the W—Ta—V_S model alloy as shown in Fig. 9. The chemical composition of the phases was also determined with TEM-EDS. A coarse particle of about 700 nm in radius was observed and it is composed of two different types of phases (see Fig. 9a). The phase in the left hand side, point" I ", has the composition of 63.7O-18.7Ta-15.0 V (at.%), which corresponds to the (Ta,V)-rich oxides as shown in the SEM image (see Fig. 4a). Phase identification was performed using selected area diffraction (SAD) and the (Ta,V)O phase has been indexed as the $TaVO_4$ phase with a tetragonal structure: a: 4.68 Å and c: 3.04 Å along the zone axis of [0−1 1], see Fig. 9b. On the other hand, the right hand side of the particle phase, see point "II", has the composition of 54.12O-42.03 V (at.%), indicating the formation of the V-rich oxide. According to the SAD pattern (see Fig. 9c), this oxide particle has been identified as the β-$V_2O_5$ phase with a monoclinic structure: a: 12.07 Å, b: 4.73 Å, c: 5.384 Å, β: 103.52 along the zone axis of [0−1 0], see Fig. 9c. It has been reported that the α-$V_2O_5$ (orthorhombic) is the most stable oxide in the V—O system; however, it can be transformed to β-$V_2O_5$ (monoclinic or tetragonal) or γ -$V_2O_5$ (orthorhombic) under high pressure and high temperature [23,24].

The small particle of about 50 nm in radius, point "III ", was also observed in the TEM image, see Fig. 9a. The nano-particle contains a high level of O, Y and Ta (the composition of 60.05O-17.80Y-12.18Ta

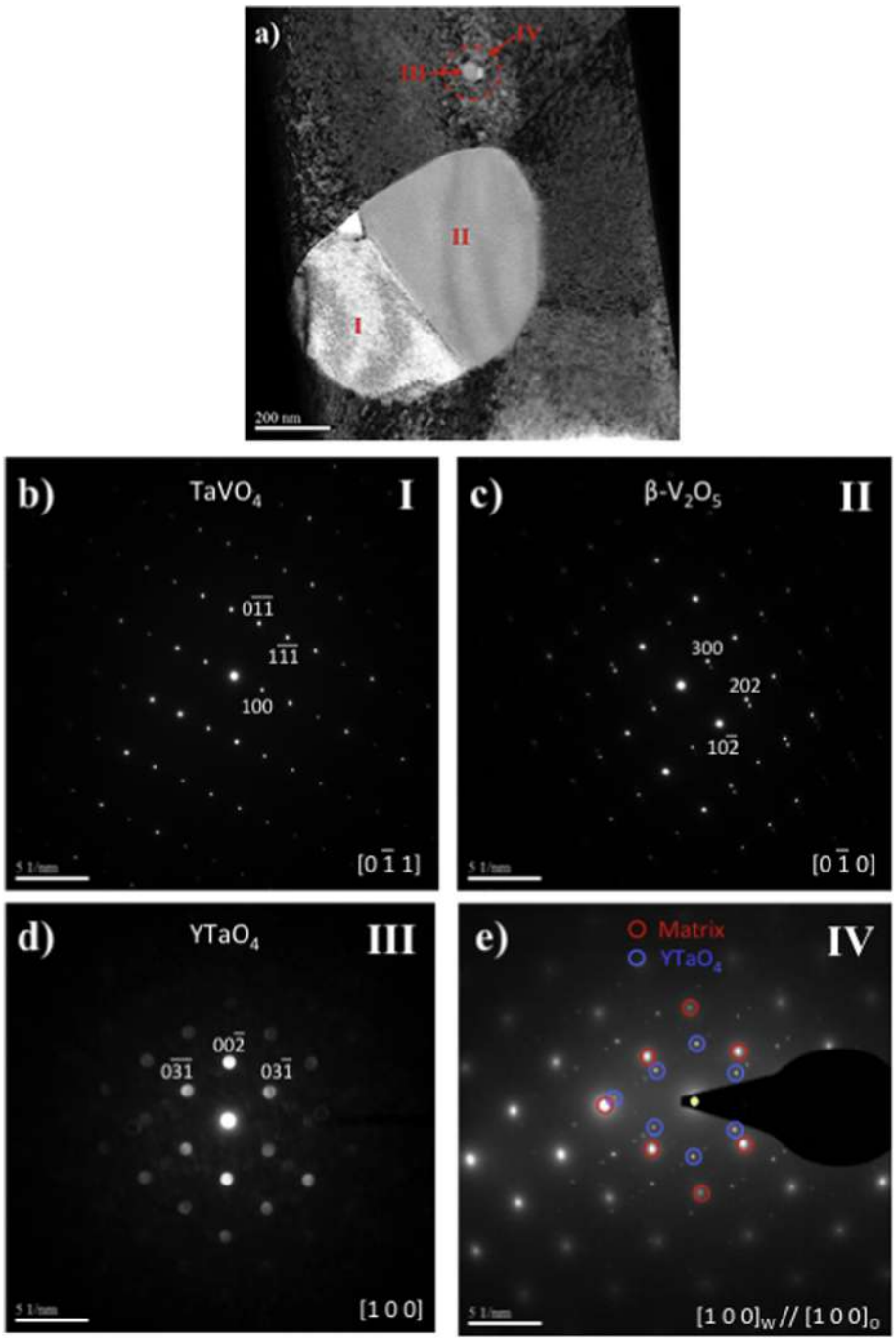


**Fig. 9.** TEM images of (a) the W–Ta–V_S model alloy and the SAD patterns of (b) the $TaVO_4$, (c) β-$V_2O_5$, (d) $YTaO_4$ and (e) W/$YTaO_4$ phases.

(at.%)). Nano-beam diffraction (NBD) has been used in phase identification of the nano-oxide particle, which has been indexed as the $YTaO_4$ phase with a monoclinic structure: a: 5.32 Å, b: 10.93 Å, c: 5.05 Å, β: 95.50 along the zone axis of [1 0 0], see Fig. 9d. In order to clarify the $YTaO_4$ oxide phase precipitated from the tungsten matrix, phase identification was performed at the region of the point "IV ", see Fig. 9a, using selected area diffraction (SAD) as shown in Fig. 9e. It demonstrates that the orientation relationship between W matrix (W, rad circle) and $YTaO_4$ oxide (O, blue circle) is $[100]_W//[100]_O$, which implied that the interface between $YTaO_4$ and W is coherent, as shown in Fig. 9e.

It is believed that the addition of Y in the tungsten matrix during the first stage of milling could promote the formation of in-situ yttrium oxide ($Y_2O_3$), which can further interact with alloying elements (Ta, V) during the secondary ball milling. In this case, the chemical bonds of Y–Ta–O elements might easily occur and form the monoclinic $YTaO_4$ phase as the interaction of the $Y_2O_3/Ta_2O_5$ oxides during the process of mechanical alloying. The existence of the strain energy during the collision-friction energy in ball-milling process facilitates the nucleation of the $YTaO_4$ phase by forming coherent interface on the tungsten matrix. It should be pointed out that in-situ formed dispersoids can effectively inhibit movement of dislocations and pin migration of grain boundaries, which increase the resistance of the alloy to creep deformation [25].

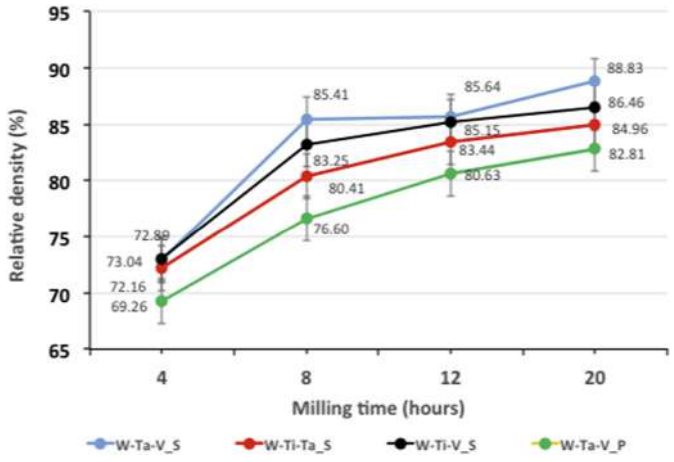


**Fig. 10.** Relative density of the sintered model alloys at different milling durations.

### 3.2.3. Relative density

Fig. 10 shows the relative density of the four model alloys at different milling time. It can be seen clearly that the relative density increases as the milling time increases, suggesting a high degree of densification can be achieved after a long milling duration. Additionally, the use of the secondary milling method has an increase in relative density compared to that of the primary milling method. The highest relative density of 89% was obtained at the W–Ta–V_S sample milled for 20 h, while the W–Ta–V_P sample is only about 83%. It should be also noted that the addition of V tends to increase the relative density of the tungsten model alloys. It has been proposed that the V element can improve the densification and mechanical properties of the tungsten based materials by mechanical alloying [10]. It is believed that the V addition could facilitate the grain refinement and homogeneity of the microstructure of tungsten alloys as shown in SEM images (Fig. 4a and c). The results indicate that the secondary milling method and the addition of V have a significant influence on the relative density of tungsten alloys. It should be also mentioned that the relative density of the model alloys obtained in this work is low (~85%), which could be attributed to the use of a conventional uniaxial compaction and a large number of oxide particle formation in the tungsten matrix.

### 3.3. Hardness and nanoindentation

Fig. 11a shows Vickers hardness of the W–Ta–V_S model alloy as a function of milling time. The results showed that hardness of the model alloy has increased as the milling time increased from 442HV at 4 h of milling to 506HV at 20 h of milling. It can be attributed that high strain energy and fine crystallite size were obtained after complete milling process, leading to grain refinement and the formation of uniform oxide particles.

Fig. 11b exhibits Vickers hardness of the four model alloys. The model alloy with the addition of Ta and V elements using secondary milling method indicates the highest hardness value (506HV). It can be ascribed to the presence of a homogeneous and dense microstructure as well as the formation of fine (Ta,V)-rich or V-rich oxide particles uniformly dispersed in the tungsten matrix. The results also suggest that the model alloy with the primary milling procedure has the lowest hardness value (418HV), which is strongly related to a large size of second phase formation and inhomogeneity of microstructure.

Nanoindentation was used to determine the hardness and elastic modulus of the tungsten model alloys milled for 20 h as listed in Table 3. The results demonstrate that W–Ta–V_S model alloy has the highest indented hardness and elastic modulus values up to 7.32 GPa and 353.1 GPa compared to other model alloys. The curves of hardness-displacement and modulus-displacement, see Fig. 12, also demonstrate that the model alloys containing V element by using secondary ball milling tend to a higher hardness and modulus; however, the lowest hardness was found in alloys with the primary ball milling. The tendency of variation is similar to the results of Vickers hardness illustrated in Fig. 11. It should be also noted that an increase in the hardness with decreasing indentation depth was clearly observed in all the model alloys, see Fig. 12. This phenomenon is commonly referred to as the indentation size effect (ISE) [26].

Fig. 13 shows a typical load-displacement curve of the W–Ta–V_S and W–Ta–V_P in a nanoindentation testing. The load-displacement curve of W–Ta–V_S describes a higher hardness and elastic modulus compared to W–Ta–V_P model alloy. The result suggests that the secondary ball milling methods with Ta and V elements could facilitate the grain refinement and microstructure homogeneity of the tungsten alloys.

**Table 3**
Hardness and elastic modulus of different model alloys measured by nanoindentation tests.

| Model Alloys | Hardness (GPa) | Elastic Modulus (GPa) |
|---|---|---|
| W–Ta–V_S | 7.32 | 353.2 |
| W–Ti–Ta_S | 7.17 | 346.2 |
| W–Ti–V_S | 7.20 | 350.4 |
| W–Ta–V_P | 6.59 | 256.5 |

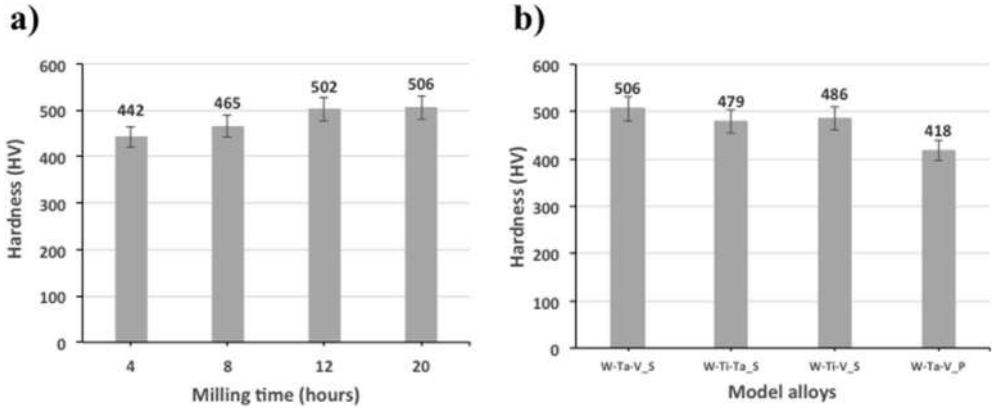


**Fig. 11.** Vickers hardness of (a) the W–Ta–V_S model alloys as a function of milling time and (b) the four different model alloys.

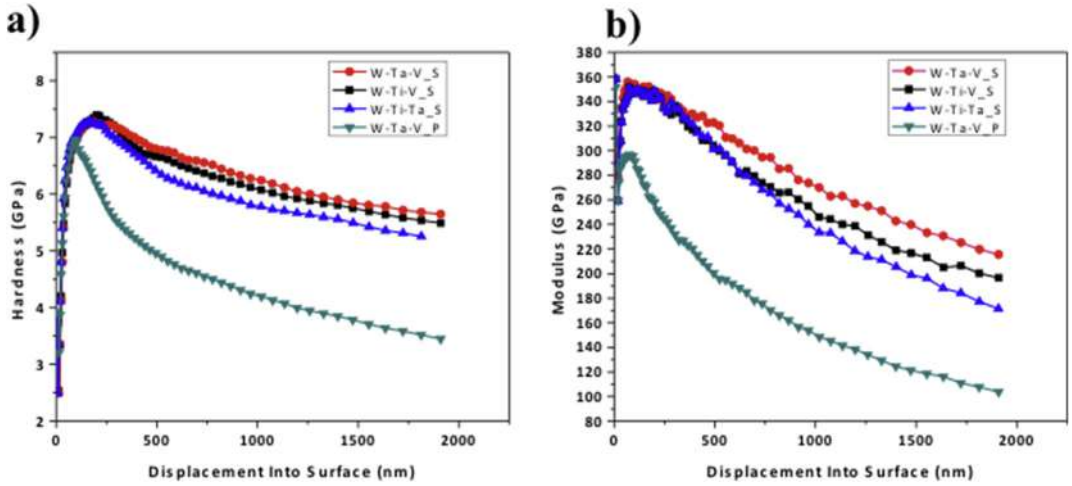


**Fig. 12.** The hardness–displacement curve of the four model alloys ~~at different milling times.~~

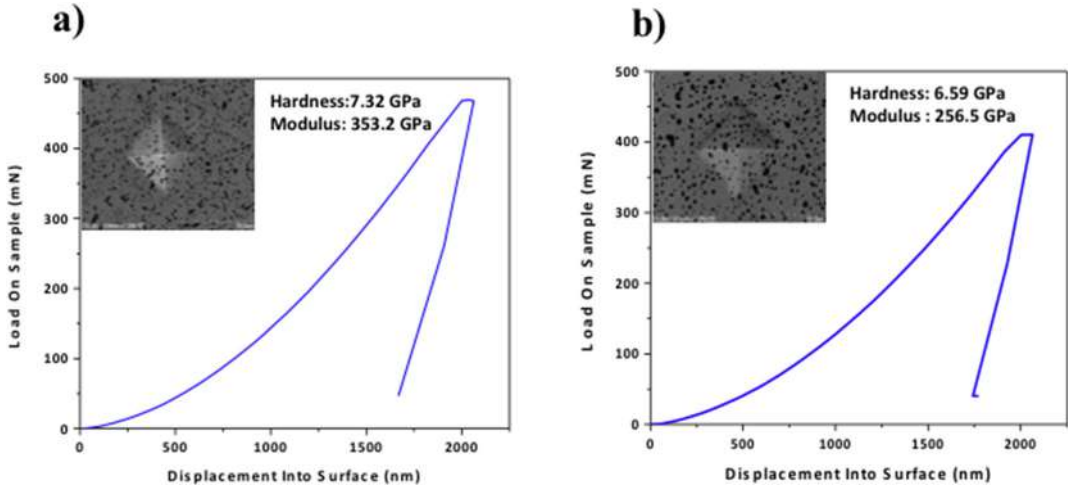


**Fig. 13.** A typical load-displacement curve of the W–Ta–V_S and W–Ta–V–P model alloys.

## 4. Conclusions

Tungsten based alloys are promising candidate materials for plasma facing components in advanced nuclear energy system. In this study, the W-(Ta,Ti,V) models alloys dispersed with in-situ yttrium oxides were synthesized by mechanical alloying. The effect of Ta, V and Ti elements on microstructure evolution and properties of the tungsten model alloys were investigated. The results show that the presence of V element can refine the second phase particles with the uniform distribution of microstructure. The addition of Ta seems to change the morphology of oxide particles from an irregular shape to a more spherical shape. Ti addition can promote the formation of a large size of Ti-rich oxide particles. The (Ta,V)-rich and V-rich oxides were found in the microstructure and have been identified as the $TaVO_4$ and $V_2O_5$ phases. The presence of Y in the tungsten matrix could promote the formation of in-situ yttrium oxide ($Y_2O_3$) and then further interacted with Ta and V during ball milling. Therefore, the $YTaO_4$ phase has been obtained by forming coherent interface on the tungsten matrix, suggesting the interaction of the $Y_2O_3$/$Ta_2O_5$ oxides during the process of mechanical alloying. Moreover, the secondary ball milling method was effective to refine the microstructure and to increase the relative density and mechanical properties.

## Declaration of competing interest

The authors declare that they have no known competing financial interests or personal relationships that could have appeared to influence the work reported in this paper.

## CRediT authorship contribution statement

**Chun-Liang Chen:** Supervision, Conceptualization, Validation, Writing - review & editing, Resources, Project administration. **Sutrisna:** Methodology, Software, Data curation, Writing - original draft, Visualization, Investigation.

## Acknowledgements

The authors would like to gratefully acknowledge financial support from Ministry of Science and Technology (MOST) Taiwan under the grant MOST 108-2221-E-259 -017 -MY2.

## References

[1] P. Norajitra, L. V Boccaccini, E. Diegele, V. Filatov, A. Gervash, R. Ruprecht, V. Slobodtchouk, Development of a helium-cooled divertor concept : design-related requirements on materials and fabrication technology 333 (2004)

1594–1598, https://doi.org/10.1016/j.jnucmat.2004.04.137.
[2] H. Bolt, V. Barabash, W. Krauss, J. Linke, R. Neu, S. Suzuki, N. Yoshida, A.U. Team, Materials for the plasma-facing components of fusion reactors, J. Nucl. Mater. 329–333 (2004) 66–73, https://doi.org/10.1016/j.jnucmat.2004.04.005.
[3] O.A. Waseem, H.J. Ryu, Tungsten-based composites for nuclear fusion applications, Nuclear Material Performance (2016), https://doi.org/10.5772/62434.
[4] I. Smid, M. Akiba, G. Vieider, L. Plöchl, Development of Tungsten Armor and Bonding to Copper for Plasma-Interactive Components, vol. 263, 2000, pp. 160–172, https://doi.org/10.1016/S0022-3115(98)00358-4.
[5] A.S. Argon, S.R. Maloof, Plastic deformation of tungsten single crystals at low temperatures, Acta Metall. 14 (1996) 1449–1462, https://doi.org/10.1016/0001-6160(66)90165-9.
[6] M. Rose, A.G. Balogh, H. Hahn, Instability of irradiation induced defects in nanostructured materials, Nucl. Instrum. Methods Phys. Res. B 127 (1997) 119–122, https://doi.org/10.1016/S0168-583X(96)00863-4.
[7] N. Nita, R. Schaeublin, M. Victoria, Impact of irradiation on the microstructure of nanocrystalline materials, J. Nucl. Mater. 333 (2004) 953–957, https://doi.org/10.1016/j.jnucmat.2004.04.058.
[8] C. Suryanarayana, E. Ivanov, V.V. Boldyrev, The science and technology of mechanical alloying, Mater. Sci. Eng. 304–306 (2001) 151–158, https://doi.org/10.1016/S0921-5093(00)01465-9.
[9] C. Suryanarayana, N. Al-Aqeeli, Mechanically alloyed nanocomposites, Prog. Mater. Sci. 58 (2013) 383–502, https://doi.org/10.1016/j.pmatsci.2012.10.001.
[10] K. Arshad, M. Zhao, Y. Yuan, Y. Zhang, Z. Zhao, B. Wang, Z. Zhou, G. Lu, Effects of vanadium concentration on the densification, microstructures and mechanical properties of tungsten vanadium alloys, J. Nucl. Mater. 455 (2014) 96–100, https://doi.org/10.1016/j.jnucmat.2014.04.019.
[11] Z. Wang, Y. Yuan, K. Arshad, J. Wang, Z. Zhou, J. Tang, G.H. Lu, Effects of tantalum concentration on the microstructures and mechanical properties of tungsten-tantalum alloys, Fusion Eng. Des. 125 (2017) 496–502, https://doi.org/10.1016/j.fusengdes.2017.04.082.
[12] K. Arshad, J. Wang, Y. Yuan, Y. Zhang, Z.J. Zhou, G.H. Lu, Development of tungsten-based materials by different sintering techniques, Int. J. Refract. Metals Hard Mater. 50 (2015) 253–257, https://doi.org/10.1016/j.ijrmhm.2015.02.004.
[13] Y. Kikuchi, I. Sakuma, D. Iwamoto, Y. Kitagawa, N. Fukumoto, M. Nagata, Y. Ueda, Surface cracking and melting of different tungsten grades under transient heat and particle loads in a magnetized coaxial plasma gun, J. Nucl. Mater. 438 (2013) 715–718.
[14] M. Wirtz, J. Linke, G. Pintsuk, L. Singheiser, I. Uytdenhouwen, Comparison of the thermal shock performance of different tungsten grades and the influence of microstructure on the damage behaviour, Phys. Scripta T T145 (2011), https://doi.org/10.1088/0031-8949/2011/T145/014058.
[15] C. Wan, S. Yu, X. Ju, W. Wang, Hydrogen trapping in helium-implanted W and W-Ta alloy : first-principles approach, J. Nucl. Mater. 508 (2018) 249–256, https://doi.org/10.1016/j.jnucmat.2018.05.050.
[16] S. Wurster, N. Baluc, M. Battabyal, T. Crosby, J. Du, C. García-Rosales, A. Hasegawa, A. Hoffmann, A. Kimura, H. Kurishita, R.J. Kurtz, H. Li, S. Noh, J. Reiser, J. Riesch, M. Rieth, W. Setyawan, M. Walter, J.H. You, R. Pippan, Recent progress in R&D on tungsten alloys for divertor structural and plasma facing materials, J. Nucl. Mater. 442 (2013) 181–189, https://doi.org/10.1016/j.jnucmat.2013.02.074.
[17] C.L. Chen, Y. Zeng, Influence of Ti content on synthesis and characteristics of W-Ti ODS alloy, J. Nucl. Mater. 469 (2016) 1–8, https://doi.org/10.1016/j.jnucmat.2015.11.018.
[18] C.L. Chen, Y. Zeng, Synthesis and characteristics of W-Ti alloy dispersed with Y2Ti2O7 oxides, Int. J. Refract. Metals Hard Mater. 56 (2016) 104–109, https://doi.org/10.1016/j.ijrmhm.2015.12.008.
[19] C. Chen, Y. Zeng, The effect of La on the synthesis and properties of a W-Ti alloy, Fusion Eng. Des. 113 (2016) 30–36, https://doi.org/10.1016/j.fusengdes.2016.10.002.
[20] C. Chen, Y. Zeng, Effect of consolidation and oxide dispersoid addition on phase formation and mechanical properties of W-Ti ODS alloy, Int. J. Refract. Metals Hard Mater. 60 (2016) 11–16, https://doi.org/10.1016/j.ijrmhm.2016.06.012.
[21] C. Suryanarayana, M.G. Norton, X-Ray Diffraction: A Practical Approach, Plenum Press, New York, 1998.
[22] C.L. Chen, C.L. Huang, Milling media and alloying effects on synthesis and characteristics of mechanically alloyed ODS heavy tungsten alloys, Int. J. Refract. Metals Hard Mater. 44 (2014) 19–26, https://doi.org/10.1016/j.ijrmhm.2014.01.007.
[23] P. Balog, D. Orosel, Z. Cancarevic, C. Sch, M. Jansen, V 2 O 5 phase diagram revisited at high pressures and high temperatures, J. Alloys Compd. 429 (2007) 87–98, https://doi.org/10.1016/j.jallcom.2006.04.042.
[24] V.P. Filonenko, I.P. Zibrov, High-pressure phase transitions of M 2 O 5 (M = V, Nb, Ta) and thermal stability of new polymorphs, Inorg. Mater. 37 (2001) 953–954.
[25] C. Suryanarayana, Mechanical alloying and milling, Prog. Mater. Sci. 46 (2001) 1–184, https://doi.org/10.1016/S0079-6425(99)00010-9.
[26] Y.V. Milman, A.A. Golubenko, S.N. Dub, Indentation size effect in nanohardness, Acta Mater. 59 (2011) 7480–7487, https://doi.org/10.1016/j.actamat.2011.08.027.